J. R. Long and M. Dincă

DOI: 10.1002/anie.200801163

Hydrogen Storage

Hydrogen Storage in Microporous Metal–Organic Frameworks with Exposed Metal Sites

*Mircea Dincă and Jeffrey R. Long**

Keywords:
bond dissociation energy · hydrogen storage · metal–H_2 binding · metal–organic frameworks · microporous materials

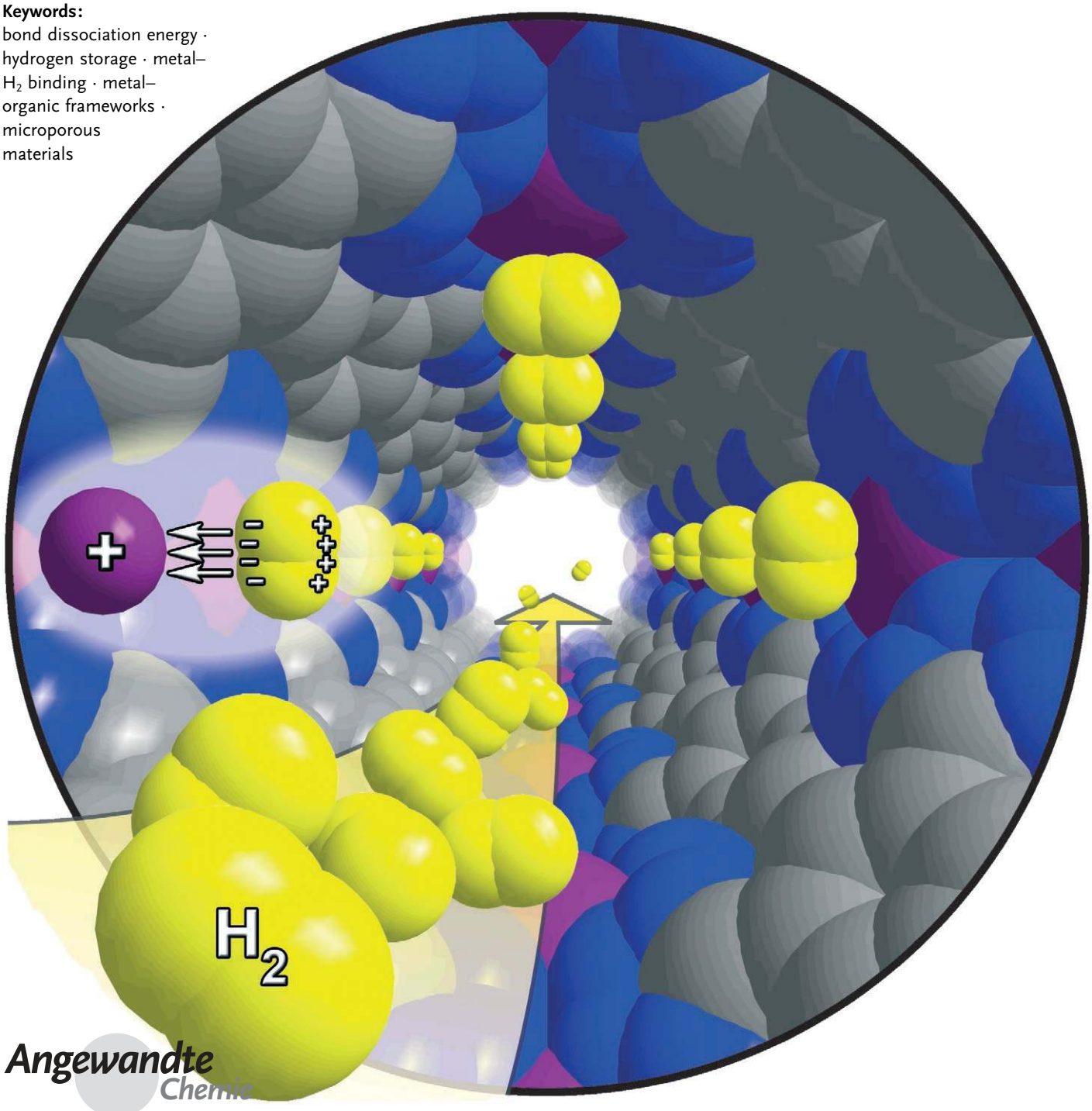

Owing to their high uptake capacity at low temperature and excellent reversibility kinetics, metal–organic frameworks have attracted considerable attention as potential solid-state hydrogen storage materials. In the last few years, researchers have also identified several strategies for increasing the affinity of these materials towards hydrogen, among which the binding of H_2 to unsaturated metal centers is one of the most promising. Herein, we review the synthetic approaches employed thus far for producing frameworks with exposed metal sites, and summarize the hydrogen uptake capacities and binding energies in these materials. In addition, results from experiments that were used to probe independently the metal–hydrogen interaction in selected materials will be discussed.

From the Contents

1. Introduction 6767
2. Hydrogen Storage Requirements 6767
3. H_2 Binding to Metal Species 6768
4. Metal–Hydrogen Binding in Metal–Organic Frameworks 6771
5. Strategies for Incorporating Unsaturated Metal Centers in Metal–Organic Frameworks 6774
6. Conclusion and Outlook 6777

1. Introduction

Hydrogen is one of the leading candidates as an energy carrier of the future because of its high energy content and clean burning, potentially renewable nature. A particularly daunting challenge facing its use in transportation, however, is the development of a safe and practical storage system. As opposed to stationary storage, in which the tank volume and mass are less of a concern, storage of large quantities of H_2 in a passenger car, for which volume, mass, and heat exchange are of utmost importance, presents a formidable scientific and engineering endeavor. Many reports have dealt with the use of hydrogen as a fuel and its storage in different solid-state media and in high-pressure or cryogenic tanks.[1] Among the newer materials, crystalline microporous solids comprised of metal building units and organic bridging ligands, known as metal–organic frameworks (MOFs), are perhaps the most promising physisorption candidates. However, because of their typically weak interaction with H_2, dominated by dispersion forces, these materials function best only at very low temperature and their use as storage media in vehicles would require cryogenic cooling.

To eliminate the need for a heavy and expensive cooling system, new ways of increasing the hydrogen affinity of these materials must be devised. In some cases, this has been achieved by minimizing the size of the pores, which enhances the van der Waals contacts with the H_2 molecules,[2] or by sequestering hydrogen inside flexible metal–organic frameworks, which then show hysteretic adsorption behavior and are able to desorb hydrogen at increased temperature.[3] Additionally, several reports have shown that coordinatively unsaturated metal centers embedded within metal–organic frameworks can participate directly in the binding of H_2, resulting in some of the highest binding energies reported thus far for high-capacity microporous materials. Given that metal–organic frameworks can be tailored to incorporate a large number of selected metal cations, this method presents a promising strategy for achieving the H_2 binding energy required for storage near room temperature.

2. Hydrogen Storage Requirements

2.1. The US DoE Storage System Targets

Recent research on hydrogen storage has been guided by the requirements set forth by the United States Department of Energy in 2003 and amended in 2006.[4] These targets were set under the assumption that future hydrogen-fueled cars should have a range of 300 miles (480 km), should operate under ambient conditions, and should allow fast, safe, and efficient fueling, similar to gasoline. Ultimately, safety concerns will limit the maximum allowed pressure for a storage device to 100 bar, meaning that solid-state materials that can be cycled at lower pressures than compressed-gas cylinders must be developed.

Because hydrogen contains three times the energy of gasoline per unit mass, it was estimated that a hydrogen storage tank would have to carry approximately 5 kg of H_2. As such, the 2010 DoE capacity targets for a fueling *system* (including the tank and its accessories) have been set at 6 wt% and 45 $g L^{-1}$ of usable H_2. The targets also specify that the system should show no decay for 1000 consecutive fueling cycles and should allow filling to full capacity in less than 3 min. The 2015 system targets are even more demanding: 9 wt% and 60 $g L^{-1}$ of H_2, 1500 cycles, and a fueling time of 2.5 min. If achieved together, these targets would lead to the same efficiency as current gasoline tanks. The immense difficulty of accomplishing the above targets becomes clear, however, when one notes that 5 kg of hydrogen occupies a volume of 56000 L under ambient conditions, and that 5 kg of liquid hydrogen would still require a 70 L cryogenic tank.

[*] M. Dincă, J. R. Long
Department of Chemistry
University of California, Berkeley
Berkeley, CA 94720-1460 (USA)
Fax: (+1) 510-643-3546
E-mail: jrlong@berkeley.edu
Homepage: http://alchemy.cchem.berkeley.edu

Moreover, both of these calculations ignore the mass and volume of the container and of the cooling system.

2.2. Adsorption Enthalpy Requirements for Physisorptive H_2 Storage

Clearly, significant innovations are necessary to build a viable hydrogen storage system. As stated before, the greatest challenge for physisorptive materials is to increase the strength of the H_2 binding interaction. Recently, Bhatia and Myers addressed this issue by employing the Langmuir equation to derive relationships between the operating pressures of a storage tank and the enthalpy of adsorption required for storage near room temperature.[5] Using P_1 and P_2 as the lower and upper bounds of the operating pressure and approximating the H_2 adsorption entropy as $\Delta S^\circ_{ads} \approx -8R$ (R = ideal gas constant), they derived Equation (1). They then used this equation to show that a microporous material operating between 1.5 and 30 bar at 298 K should have an average optimal adsorption enthalpy ΔH°_{opt} of 15.1 kJ mol^{-1}. Similarly, if P_2 is increased to 100 bar, the required average adsorption enthalpy decreases to 13.6 kJ mol^{-1}.

$$\Delta H^\circ_{opt} = T\,\Delta S^\circ_{opt} + \frac{R\,T}{2}\ln\left(\frac{P_1\,P_2}{P_0^2}\right) \quad (1)$$

In the same work, Bhatia and Myers derived Equation (2), which can be used to calculate the optimal operating temperature T_{opt} of a hydrogen storage material for a given average enthalpy of adsorption ΔH°_{ads}. This relationship can be used to show that a microporous material with $\Delta H^\circ_{ads} = 6$ kJ mol^{-1}, which is a typical value for current metal–organic frameworks and other microporous solids, can operate between 1.5 and 100 bar at an optimal temperature of 131 K.

$$T_{opt} = \frac{\Delta H^\circ_{ads}}{[\Delta S^\circ_{ads} + (R/2)\ln(P_1\,P_2/P_0^2)]} \quad (2)$$

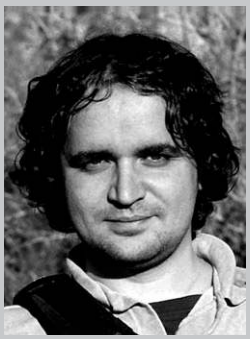

Mircea Dincă was born in Făgăras (Romania) in 1980. He received his Bachelor's Degree in Chemistry from Princeton University in 2003 working with Prof. Jeffrey Schwartz. Later that year, he joined Prof. Jeffrey R. Long's group at the University of California in Berkeley, where he is completing his PhD on the design and synthesis of microporous metal–organic frameworks for applications in gas storage, gas separation, and catalysis.

Jeffrey R. Long was born in Rolla, Missouri (USA) in 1969. He received a Bachelor's Degree in Chemistry from Cornell University in 1991 and a PhD in Chemistry from Harvard University in 1995. Following postdoctoral work at Harvard and the University of California, Berkeley, he joined the faculty in Chemistry at Berkeley in 1997. His research involves the synthesis of new inorganic clusters and solids with emphasis on magnetic and microporous materials.

3. H_2 Binding to Metal Species

As the simplest known chemical compound, the hydrogen molecule has been the subject of countless experiments and theoretical investigations, leading to some of the most fundamental discoveries in the areas of electronic structure and chemical bonding. Although metal complexes with other relatively unreactive small molecules, such as N_2, $H_2C{=}CH_2$, and even CO_2, had been known for many years,[6] the first metal complex of an H_2 molecule was not isolated until 1984, when Kubas and co-workers reported the now famous "Kubas complex" $[W(CO)_3(P\mathit{i}Pr_3)(H_2)]$ (iPr = isopropyl).[7] Using single-crystal neutron diffraction and a variety of other techniques, they later showed that this complex contained a side-on bound H_2 ligand with an H–H distance only slightly elongated relative to that in gaseous H_2, thus unequivocally proving that the complex was not a classical dihydride.[8] Subsequent to this seminal discovery, σ-H_2 complexes of virtually every transition metal have been reported, and their properties and reactivity have been the subject of many excellent review articles and a comprehensive book by Kubas.[9]

Surprisingly, despite the large number of σ-H_2 complexes that have been reported so far, the vast literature on the subject contains very few studies that address the thermodynamic properties of the metal–H_2 interaction, and in particular the bond dissociation energy (BDE) of the metal–H_2 bond. Vibrational spectroscopy, variable-temperature NMR spectroscopy, or photoacoustic calorimetry have been used to quantify this interaction in only a handful of organometallic complexes (Table 1). The BDE values obtained for many of these complexes are affected by the fleeting formation of solvento species or by the presence of agostic C–H interactions. For example, formation of the transient complex $[(C_6H_5Me)Cr(CO)_2(Xe)]$ allowed only an approximate measurement of the energy of dissociation of H_2 from $[(C_6H_5Me)Cr(CO)_2(H_2)]$, which was estimated at 70 kJ mol^{-1}.[27] The energy of the agostic C–H interaction, which affects particularly the complexes containing trialkylphosphine ligands, is also notoriously difficult to measure, and BDE values obtained for the respective σ-H_2 complexes are likely underestimated by around 40 kJ mol^{-1}.[9b]

Despite the experimental difficulties associated with measuring BDE values for organometallic σ-H_2 complexes, certain trends can be observed from selected series of isoelectronic compounds, such as $[M(CO)_3(PCy_3)_2(H_2)]$ (M = Cr, Mo, W). BDE values of 31(4), 27.2(8), and 39(4), obtained for the respective Cr, Mo, and W complexes, indicate that the strength of the metal–H_2 interaction varies as in the order Cr ≈ W > Mo.[28,38,45] However, qualitative stability studies for complexes of other transition metals

Table 1: Experimentally determined values for the $M-H_2$ bond dissociation energy (BDE) in metal species with the general formula $[M(H_2)_n]$.

M[a]	$M-H_2$ bond dissociation energy [kJ mol^{-1}]						Ref.
	n						
	1	2	3	4	5	6	
H^+-SSZ13	9.7(3)						[10]
Li^+	27(19)						[11]
Li^+-ZSM5	6.5(5)						[12]
Li^+-FER	4.1(8)						[13]
Na^+	10.3(8)	9.4(8)					[14]
Na^+-ZSM5	10.3(5)						[15]
Na^+-FER	6.0(8)						[13]
Na^+-ETS10	8.7(5)						[16]
Mg^{2+} (MgO)	7.5 (C.N. = 3)						[17]
	4.6 (C.N. = 4)						
	3.6 (C.N. = 5)						
Mg^{2+}-Y	18(1)						[18]
K^+	6.1(8)	5.3(8)					[14]
K^+-ZSM5	9.1(5)						[15]
K^+-FER	3.5(8)						[13]
Sc^+	23(1)[b]	27(2)	23(1)	21(3)			[19]
Ti^+	31(2)	41(3)	39(3)	36(2)	34(2)	36(2)	[20]
V^+	43(2)	45(2)	37(2)	38(2)	18(2)	40(2)	[21]
$[V(H_2O)]^+$	41(2)	36(2)	29(3)				[21]
$[V(H_2O)_2]^+$	28(6)						[21]
$[(C_5H_5)V(CO)_3]$	91(20)						[22]
Cr^+	32(2)	38(2)	20(2)	14(2)	6(2)	5(2)	[23]
$[Cr(CO)_5]$	63(5)[c]						[24]
	78(4)[d]						[25]
$[(C_6H_6)Cr(CO)_2]$	60(4)						[26]
$[(C_6H_5Me)Cr(CO)_2]$	70[e]						[27]
$[Cr(CO)_3(PCy_3)_2]$	31(4)[f]						[28]
Mn^+	8(2)	7(2)	5.9	5.0			[29]
$(MnH)^+$	30(2)	20(2)					[29]
Fe^+	45(3)	66(3)	31(2)	36(2)	9(1)	10(1)	[30]
Co^+	75(4)	71(3)	40(2)	40(3)	18(3)	17(3)	[31]
$[(C_5H_5)Co]^+$	67.8	70.3	3.8				[32]
Ni^+	72(1)	74(1)	47(1)	30(1)	18(1)	3(1)	[33]
Cu^+	64(4)	70(4)	37(2)	21(3)	4(1)	4(1)	[34]
$[Cu(H_2O)]^+$	82(4)	16(2)					[34]
Cu_2^+	52(4)	42(1)	21(1)	15.9(8)	8.8(4)	7.1	[35]
Cu^{2+} $(Cu_3(btc)_2)$	10.1(7)						[36]
Zn^+	16(2)	12(2)	10(2)	7(2)	6(2)	5.9	[29]
Zr^+	61(1)[b]	45(1)	42(1)	38(2)	39(2)	37(2)[g]	[37]
$[Mo(CO)_5]$	81(4)						[25]
$[Mo(CO)_3(PCy_3)_2]$	27.2(8)[f]						[38]
$[RuHCl(CO)(PiPr_3)_2]$	32.2(8)[f]						[39]
$[OsHCl(CO)(PiPr_3)_2]$	59.0(8)[f]						[40]
trans-$[IrHCl_2(PiPr_3)_2]$	29.7(8)[f]						[41]
$[Ir(H)_2X(PtBu_2Me)]$	29(1) (X = Cl^-)	33(4) (X = Br^-)	39(1) (X = I^-)				[42]
$[IrH(bq)(PPh_3)_2]^+$	13.2[f]						[43]
$[W(CO)_5]$	> 67						[44]
$[W(CO)_3(PCy_3)_2]$	39(4)[f]						[38, 45]
$[W(CO)_3(PiPr_3)_2]$	47(2)[f]						[46]

[a] Abbreviations: SSZ13 = chabazite-type zeolite (Si/Al = 11.6); ZSM5 = Mobil Synthetic Zeolite-5 (Si/Al = 40); FER = ferrierite with the general chemical formula $(K,Na)_2Mg(Si,Al)_{18}O_{36}\cdot 9H_2O$; ETS10 = titanosilicate $Na_2Si_5TiO_{13}$; C.N. = coordination number; Y = zeolite Y with the general formula $0.9\pm0.2\,Na_2O\cdot Al_2O_3\cdot 4.5\pm1.5\,SiO_2$; Cy = cyclohexyl; *i*Pr = isopropyl; *t*Bu = *tert*-butyl; bq = benzoquinolinate. [b] Attachment of H_2 occurs via oxidative addition. [c] Obtained by transient infrared spectroscopy. [d] Obtained by photoacoustic calorimetry. [e] Value affected by a transient $[(C_6H_5Me)Cr(CO)_2(Xe)]$ species in the Xe matrix. [f] Value is likely underestimated by ca. 40 kJ mol^{-1}, which corresponds to the agostic C–H interaction in the H_2-free fragment.[9] [g] The BDE for a seventh hydrogen molecule attached to $[Zr(H_2)_6]^+$ is estimated to be 36(3) kJ mol^{-1}.

showed that hydrogen does not always bind to first- and third-row transition metals more strongly than to second-row metals. Indeed, the extent to which $\sigma(H_2)\rightarrow M$ donation and $M\rightarrow\sigma^*(H_2)$ back-donation contribute to the overall metal–H_2 bonding picture is not dictated only by the metal center, but also by the surrounding ligand system, which is thereby responsible for the varying trends observed for $[M(CO)_3(PCy_3)_2(H_2)]$ and other systems.[9]

Notably, gas-phase experiments have also allowed the determination of the BDE for the M–H_2 bond in a series of first-row transition-metal species with the general formula $[M(H_2)_n]^+$ (M = Sc, Ti, V, Cr, Mn, Fe, Co, Ni, Cu, Zn; $n = 1$–6). Although these systems are not ideal models for the unsaturated metal centers in metal–organic frameworks, they can nevertheless serve as informative starting points for the design of successful hydrogen storage materials; their properties are also listed in Table 1. It is interesting to note, for example, that the monovalent alkali metal cations have much lower gas-phase H_2 binding energies of 10.3 kJ mol^{-1} and 6.1 kJ mol^{-1}, for Na^+ and K^+, respectively, than the transition-metal cations, which, with the exception of Mn^+ and Zn^+, have M^+–H_2 BDEs ranging from 23 kJ mol^{-1} for Sc^+ to 75 kJ mol^{-1} for Co^+. This difference has been assigned to the fact that the closed-shell configuration of alkaline-metal ions does not allow for back-donation into the σ* orbital of the H_2 molecule. As stated before, the back-donation interaction is responsible for part of the H_2 binding picture in side-on H_2 complexes, and, if manifested prominently, it can lead to oxidative addition of H_2 to the metal fragment with the concomitant formation of a classical dihydride.[9]

Somewhat counterintuitively, the gas-phase measurements also revealed that the BDE typically increases from $n = 1$ to $n = 2$ for the transition-metal ions. This initial increase has been attributed to the mixing between the 3dσ orbital and the empty 4s orbital, which is already present in the $[M(H_2)^+]$ species. The typically linear geometry of the $[M(H_2)_2^+]$ species allows both H_2 ligands to share the cost of the hybridization, giving a larger BDE to the second H_2 molecule.[29] A mild decrease in the BDE is observed with further increase of n for all transition-metal ions, which has been associated with a decrease in the σ-accepting abilities of the polyhydrogenated metal species. Importantly, this trend also suggests that unsaturated metal sites within metal–organic frameworks, which are typically surrounded by three, four, or five ligands of better σ-donating ability than H_2, are expected to exhibit even lower H_2 affinities than the respective $[M(H_2)_3^+]$, $[M(H_2)_4^+]$, and $[M(H_2)_5^+]$ species.

In addition to the studies of molecular metal–H_2 species, a large body of literature is dedicated to the interaction of H_2 with metal surfaces. Although molecular hydrogen is typically short-lived and dissociates at the surface of most metals, low temperature experiments and direct calorimetric measurements have allowed the characterization of a relatively large number of these fleeting interactions. Reported values for the enthalpy of H_2 adsorption to metal surfaces range from 39 and 42 kJ mol^{-1} for Cu(311) and Pt(111), respectively, to 142 and 155 kJ mol^{-1} for the (110) and (111) surfaces of Mo and W, respectively.[47]

Perhaps the most relevant experimental BDE values for the design of new frameworks for hydrogen storage have come only recently with the measurement of metal–H_2 interactions in ion-exchanged zeolites.[12,13,15] Temperature-dependent infrared spectroscopy was used to determine the interaction energy of H_2 with Li^+, Na^+, and K^+ ions in zeolites ZSM-5 and ferrierite, and showed that Na^+ consistently binds H_2 more strongly than do Li^+ and K^+. On the other hand, the study also suggests that none of these cations could provide the 13–15 kJ mol^{-1} necessary for room-temperature hydrogen storage. However, the fact that Mg^{2+}-exchanged zeolite Y showed an H_2 adsorption enthalpy of 18 kJ mol^{-1} suggests that use of cations with no back-donation abilities, but with higher formal charges increases the electrostatic interaction with H_2 and may lead to materials with optimal H_2 binding energies.

Although limited, the data summarized in Table 1 allow several important conclusions to be made regarding metal-H_2 binding for hydrogen storage. First, incorporation of alkali-metal cations in metal–organic frameworks is unlikely to lead to materials with H_2 binding energies fit for room-temperature storage. Instead, the experimental data show that the transition metals display a much wider range of H_2 affinities, some of which fall in the desired 15–20 kJ mol^{-1} range. Moreover, gas-phase measurements for monovalent cations indicate that one could benefit especially from the use of Co^+, Ni^+, and Cu^+ species, which display stronger initial H_2 binding energies than other ions. Importantly, however, data reported for organometallic complexes suggest that the H_2 binding energy characteristic of low-valent metals is too high for room-temperature applications and that novel means of incorporating metals with higher oxidation states and diminished back-donation abilities need to be found. In addition, the design of metal–organic frameworks with coordinatively unsaturated metal centers must take into account the weight of the metals used, thereby narrowing the available candidates to first-row transition metals and light, high-valent main-group cations such as Mg^{2+}, Ca^{2+}, Al^{3+}, and Ga^{3+}.

In the absence of a more extended pool of experimental results, theoretical investigations of H_2 binding to metals could also contribute significantly to the design of new hydrogen storage materials. Numerous computational studies have already modeled H_2 interactions with single metal ions, metal surfaces, and organometallic σ-H_2 complexes.[48] For example, Lochan and Head-Gordon recently used DFT calculations to address the issue of H_2 binding to gas-phase Li^+, Na^+, Mg^{2+}, and Al^{3+} ions and found that the strength of H_2 binding increases with increasing charge owing to the electrostatic interactions.[49] Computational investigations have also unveiled new structures that could exhibit excellent H_2 storage properties, such as alkali-metal- and Ti-decorated fullerenes,[50] and even Li-doped metal–organic frameworks.[51] Synthesis of such materials, however, is likely to be difficult because of the expected bulk phase instability of many of the proposed structures.

Computational studies that model the metal–H_2 interaction in metal–organic frameworks are also exceedingly scarce and have thus far relied mostly on grand canonical Monte Carlo simulations and ab initio calculations.[52] The difficulty of dealing with these complex solid-state systems is accen-

tuated by the fact that open-shell electronic configurations and negative charge considerations often make DFT calculations computationally demanding and unreliable. As such, the issue of modeling the H_2 interaction with coordinatively unsaturated metal centers within metal–organic frameworks still represents an important and largely unsolved problem.

4. Metal–Hydrogen Binding in Metal–Organic Frameworks

Infrared spectroscopy provided the first experimental evidence of H_2 binding to a metal center inside a metal–organic framework. Bordiga, Zecchina, and co-workers showed that H_2 adsorbed into $Cu_3(btc)_2$ displays an infrared stretching band at 4100 cm^{-1}, which is characteristic of metal–H_2 interactions.[53] Low-temperature powder neutron diffraction experiments later verified that D_2 binds to the empty, axial coordination sites of the Cu_2–tetracarboxylate paddlewheel building units (Figure 1), and showed that the Cu^{2+}–D_2 distance is 2.39 Å.[54] This distance is somewhat longer than the Mn^{2+}–D_2 distance of 2.27 Å in $Mn_3[(Mn_4Cl)_3(btt)_8(CH_3OH)_{10}]_2$ (Figure 2), for which D_2 binding to the square-planar Mn_4Cl units was also probed by powder neutron diffraction.[55] The difference between the two M^{2+}–D_2 distances agrees well with the observation that H_2 binds more strongly in the Mn^{2+} compound than in the Cu^{2+} compound, which show zero-coverage enthalpies of adsorption of 10.1 and 6.8 kJ mol^{-1}, respectively.[55,56]

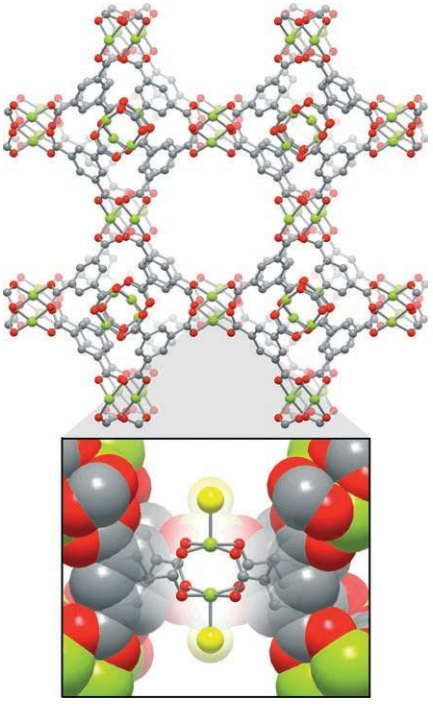

Figure 1. A portion of the crystal structure of $Cu_3(btc)_2$ and the position of the Cu^{2+}-bound D_2 molecules (yellow spheres) as determined by powder neutron diffraction. Green, red, and gray spheres represent Cu, O, and C atoms, respectively. Hydrogen atoms omitted for clarity.

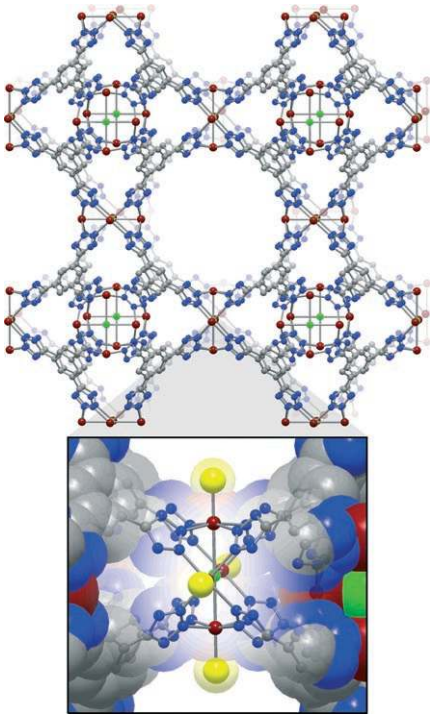

Figure 2. A portion of the crystal structure of $Mn_3[(Mn_4Cl)_3(btt)_8(CH_3OH)_{10}]_2$ and the position of the Mn^{2+}-bound D_2 molecules (yellow spheres) as determined by powder neutron diffraction. Maroon, green, blue, and gray spheres represent Mn, Cl, N, and C atoms, respectively. Hydrogen atoms and methanol molecules are omitted for clarity.

Metal–H_2 interactions in microporous frameworks have been directly observed in only five other cases so far, and the hydrogen storage properties of these materials are also summarized in Table 2. For example, powder neutron diffraction experiments were employed to detect Cu^{2+}–D_2 interactions in the Prussian blue analogue $Cu_3[Co(CN)_6]_2$[64] and in $HCu[(Cu_4Cl)_3(btt)_8]\cdot 3.5\,HCl$,[65] a sodalite-type framework isostructural with the Mn^{2+} compound displayed in Figure 2. Whereas the unsaturated Cu^{2+} sites in the Prussian blue analogue were observed to bind D_2 only at increased D_2 loading, five-coordinate Cu^{2+} ions were identified as the strongest adsorption sites in the sodalite-type framework, in which Cu^{2+}–D_2 distances of 2.47 Å were observed. As in $Cu_3(btc)_2$, the Jahn–Teller effect is likely to be responsible for this somewhat longer Cu^{2+}–D_2 distance and the lower zero-coverage H_2 binding enthalpy of 9.5 kJ mol^{-1} relative to the Mn^{2+} analogue. However, in contrast to $Mn_3[(Mn_4Cl)_3(btt)_8(CH_3OH)_{10}]_2$, for which methanol molecules occupy approximately 80% of the Mn^{2+} sites, neutron diffraction confirmed that all of the Cu^{2+} sites were available for D_2 binding in $HCu[(Cu_4Cl)_3(btt)_8]\cdot 3.5\,HCl$. The complete desolvation of the Cu^{2+} sites resulted in a larger enthalpy of adsorption over the entire dosing pressure range, such that the Cu^{2+} analogue is expected to desorb H_2 at a higher temperature than the Mn^{2+} analogue.[65]

A very recent neutron diffraction experiment has also allowed the identification of Zn^{2+}–H_2 interactions within the microporous framework $Zn_2(dhtp)$ (dhtp = 2,5-dihydroxyterephthalate).[103] In this material, the Zn^{2+}–D_2 distance was

Table 2: Summary of porosity data and hydrogen storage properties for microporous frameworks in which H_2 binding to unsaturated metal centers has been unambiguously demonstrated by an independent technique.

Material[a]	SA_{BET} [$m^2 g^{-1}$][a]	$SA_{Langmuir}$ [$m^2 g^{-1}$][a]	H_2 uptake at 77 K [wt%]	Pressure [bar]	Max. ΔH_{abs} [$kJ mol^{-1}$]	Ref.
$Mn_3[(Mn_4Cl)_3(btt)_8(CH_3OH)_{10}]_2$	2057	2230	2.23	1.2	10.1	[55]
			5.1 (6.9[b])	90		
$NaNi_3(OH)(sip)_2$	700		0.94	1	10.4	[57]
$Ni_{20}(OH)_{12}[(HPO_4)_8(PO_4)_4]$	500		0.53	0.79		[58, 59]
$Cu_3(btc)_2$	1507	2175	2.5	1	6.8[c]	[56]
	1944	2257	3.26	77		[60]
		872	1.38	0.92		[53]
			1.44	1	6.6	[61]
			2.27	1		[62]
			3.6	10		
	1154		3.6	70	4.5	[63]
$Cu_3[Co(CN)_6]_2$[d]	730		1.8	1.2	7.0	[64]
$HCu[(Cu_4Cl)_3(btt)_8]\cdot 3.5HCl$	1710	1770	4.2 (5.7[b])	90	9.5	[65]
$Zn_2(dhtp)$	783	1132	1.77/2.3	1/26	8.3	[56]
	870		2.8	30	8.8	[103]

[a] Abbreviations: SA = apparent surface area; btt = 1,3,5-benzenetristetrazolate; sip = 5-sulfoisophthalate; btc = 1,3,5-benzenetricarboxylate; dhtp = 2,5-dihydroxyterephthalate. [b] Total adsorption values. [c] The adsorption enthalpy at an isolated Cu^{2+} center is estimated to be 10.1(7) $kJ mol^{-1}$.[36] [d] Adsorption at the unsaturated Cu^{2+} sites was observed only at higher D_2 loadings.

estimated to be 2.6 Å, a somewhat larger value than those observed for Mn^{2+} and Cu^{2+}, which likely contributes to the comparatively low initial binding energy of 8.8 $kJ mol^{-1}$.[103] Notably, very short D_2–D_2 distances of only 2.85 Å were observed within the first adsorbed layer, suggesting that the presence of unsaturated metal sites can indeed increase the packing efficiency of H_2 within microporous frameworks relative to even solid hydrogen, which exhibits intermolecular distances of 3.6 Å.[103]

In two other experiments, inelastic neutron scattering (INS) spectroscopy was used to prove Ni^{2+}–D_2 interactions in the microporous nickel phosphate $Ni_{20}(OH)_{12}[(HPO_4)_8(PO_4)_4]$[58] and in the nickel sulfoisophthalate $NaNi_3(OH)(sip)_2$.[57] As shown in Figure 3, the isophthalate framework has three crystallographically independent nickel atoms, two of which are coordinated by water molecules, which can be evacuated to give unsaturated Ni^{2+} sites. Although the INS experiments indicated metal–D_2 interactions that were subsequently attributed to the Ni^{2+} ions, it is possible that further experiments would also reveal D_2 binding to the Na^+ ions, which initially possess two terminal water ligands. As shown in Table 1 and discussed in Section 3, however, the Na^+–H_2 interaction is expected to be much weaker than the Ni^{2+}–H_2 interaction, which therefore ought to be almost entirely responsible for the high zero-coverage H_2 binding energy of 10.4 $kJ mol^{-1}$ observed in $NaNi_3(OH)(sip)_2$.[57]

The relatively large enthalpies of adsorption observed in the aforementioned compounds have positive effects on their hydrogen uptake capacities. For example, $Mn_3[(Mn_4Cl)_3(btt)_8(CH_3OH)_{10}]_2$ exhibits a total H_2 adsorption capacity of 6.9 wt% at 90 bar and 77 K, which corresponds to a volumetric capacity of 60 $g L^{-1}$, only 11 $g L^{-1}$ lower than the density of liquid H_2 at 20 K. As mentioned before, the metal–H_2 distances in this material are at least 1 Å shorter than typical van der Waals contacts, which are normally greater than 3.3 Å. This result suggests that H_2 molecules pack more efficiently inside pores lined with unsaturated metal centers, proving that this approach is a key strategy for achieving high volumetric storage density. By comparison, $[Mn(dmf)_6]_3[(Mn_4Cl)_3(btt)_8(dmf)_{12}]_2$, the isomorphous framework in which the coordination spheres of all Mn^{2+} ions are saturated by DMF molecules and the zero-coverage enthalpy of adsorption is only 7.6 $kJ mol^{-1}$, adsorbs a total of only 3.9 wt% at 50 bar and 77 K.[55]

The positive influence of the unsaturated metal sites becomes evident especially when comparing the room temperature adsorption capacities of the frameworks in Table 3 with the results obtained for the best metal–organic frameworks without unsaturated metal sites. The current records for low-

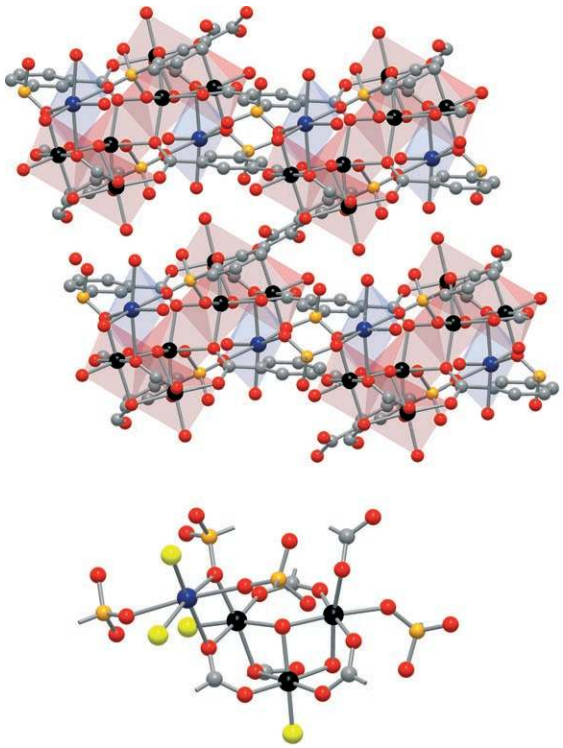

Figure 3. A portion of the crystal structure of $NaNi_3(OH)(sip)_2$ and the building unit of this material. Yellow spheres represent the potential positions of D_2 binding as suggested by inelastic neutron scattering. The positions of the D_2 molecules were generated by replacing the bound water molecules, as determined by X-ray crystallography. Black, dark blue, orange, red, and gray spheres represent Ni, Na, S, O, and C atoms, respectively. Hydrogen atoms are omitted for clarity.

Table 3: Porosity data and H_2 storage properties for microporous metal–organic frameworks with coordinatively unsaturated metal centers.[a]

Material[b]	Metal building unit formula (Figure 4)	SA_{BET}[c] [$m^2 g^{-1}$]	$SA_{Langmuir}$[c] [$m^2 g^{-1}$]	H_2 uptake [wt%, 77 K]	P [bar]	ΔH_{ads} [$kJ mol^{-1}$]	Ref.
$Li_{3.2}Mn_{1.4}[(Mn_4Cl)_3(btt)_8]_2$·0.4 LiCl	$Mn_4(\mu_4\text{-Cl})(N_4CR)_8$ (**7**)	1904	2057	2.06	1.2	8.9	[68]
$Li^+@Zn_2(ndc)_2(diPyNI)$	Li^+ intercalation	756		1.63	1	6.1	[69]
$Mg_3(ndc)_3$	$Mg_3(O_2CR)_6$ (**6**)	10[d]		0.46	1.2	9.5	[70]
			520	0.78	1		[71]
$Al_{12}O(OH)_{18}[Al_2(OH)_4](btc)_6$	$Al_3(\mu_3\text{-O})(O_2CR)_6$ (**4**)			1.91[e]	3		[72]
$Cr_3OF(btc)_2$	$Cr_3(\mu_3\text{-O})(O_2CR)_6$ (**4**)		2700	3.3	25	6.3	[73]
$Cr_3OF(bdc)_3$	$Cr_3(\mu_3\text{-O})(O_2CR)_6$ (**4**)		5900	4.5	30		[73]
			5500	6.1	60	10.0	[74]
$Cr_3OF(ntc)_{1.5}$	$Cr_3(\mu_3\text{-O})(O_2CR)_6$ (**4**)		42	1.0	35	6.0	[75]
$Mn_3(bdt)_3$	$Mn_3(N_4CR)_6$ (**5**)	290		0.97	1.2	8.4	[76]
$Mn_2(bdt)Cl_2$	$Mn_2(\mu\text{-Cl})(\mu\text{-}N_4CR)$ (**15**)	530		0.82	1.2	8.8	[76]
Mn(ndc)	$Mn(\mu\text{-}O_2CR)$ chains (**11**)	191		0.57	1		[77]
$Mn_3[(Mn_4Cl)_3(tpt\text{-}3tz)_8(dmf)_{12}]_2$[f]	$Mn_4(\mu_4\text{-Cl})(N_4CR)_8$ (**7**)	1580	1700	3.7 (4.5[g])	80	7.6	[78]
$Fe_3[(Mn_4Cl)_3(btt)_8]_2$·$FeCl_2$	$Mn_4(\mu_4\text{-Cl})(N_4CR)_8$ (**7**)	2033	2201	2.21	1.2	10.2	[68]
$Fe_4O_2(btb)_{8/3}$	$Fe_4(\mu_3\text{-O})_2(O_2CR)_8$ (**9**)	1121	1835	2.1	1		[79]
$Fe_3O(F_4bdc)_3$	$Fe_3(\mu_3\text{-O})(O_2CR)_6$ (**4**)		635	0.9	1		[80]
$H_2[Co_4O(tatb)_{8/3}]$	$Co_4(\mu_4\text{-O})(O_2CR)_8$ (**8**)		1355	1.53	1	10.1	[81]
$Co_3[(Mn_4Cl)_3(btt)_8]_2$·$1.7CoCl_2$	$Mn_4(\mu_4\text{-Cl})(N_4CR)_8$ (**7**)	2096	2268	2.12	1.2	10.5	[68]
$Ni_{2.75}Mn_{0.25}[(Mn_4Cl)_3(btt)_8]_2$	$Mn_4(\mu_4\text{-Cl})(N_4CR)_8$ (**7**)	2110	2282	2.29	1.2	9.1	[68]
$Ni_2(dhtp)$	$Ni(\mu\text{-}O_2CR,O)$ chains (**10**)		1083	1.8	70		[82]
$H_2[Ni_3O(tatb)_2]$	$Ni_3(\mu_3\text{-O})(O_2CR)_6$ (**4**)		225	0.63[e]	1		[83]
$Cu_2(bptc)$	$Cu_2(O_2CR)_4$ (**1**)		1830	2.47	1		[84]
		1670		2.59/4.20	1/20		[85]
$Cu_2(tptc)$	$Cu_2(O_2CR)_4$ (**1**)	2247		2.52/6.06	1/20		[85]
$Cu_2(qptc)$	$Cu_2(O_2CR)_4$ (**1**)	2932		2.24/6.07	1/20		[85]
Cu(bdt)·0.25DMF	$Cu(\mu\text{-}N_4CR)_2$ chains (**14**)	200[d]		0.66	1.2		[76]
$Cu_3(tatb)_4$ (noncatenated)	$Cu_2(O_2CR)_4$ (**1**)		2700	1.62	1		[86]
$Cu_3(tatb)_4$ (catenated)	$Cu_2(O_2CR)_4$ (**1**)		3800	1.9	1		[87]
Cu_3(BPTriC)	$Cu_2(O_2CR)_4$ (**1**) and $Cu_3(O_2CR)_6$ (**4**) (no μ_3-O)	2300	3100	5.7	45	7.3	[88]
$Cu_6O(tzi)_3(NO_3)$	$Cu_2(O_2CR)_4$ (**1**) and $Cu_3(\mu_3\text{-O})(N_4CR)_3$ (**3**)	2847	3223	2.4	1	9.5	[89]
$Cu_3[(Cu_4Cl)_3(tpb\text{-}3tz)_8]_2$·$11CuCl_2$	$Cu_4(\mu_4\text{-Cl})(N_4CR)_8$ (**7**)	1120	1200	2.8	30	8.2	[78]
$Mn_3[(Mn_4Cl)_3(btt)_8]_2$·$0.75CuPF_6$	$Mn_4(\mu_4\text{-Cl})(N_4CR)_8$ (**7**)	1911	2072	2.00	1.2	9.9	[68]
$Cu_3[(Cu_{2.9}Mn_{1.1}Cl)_3(btt)_8]_2$·$2CuCl_2$	$Mn_4(\mu_4\text{-Cl})(N_4CR)_8$ (**7**)	1695	1778	2.02	1.2	8.5	[68]
$Zn_3[(Zn_{0.7}Mn_{3.3}Cl)_3(btt)_8]_2$·$2ZnCl_2$	$Mn_4(\mu_4\text{-Cl})(N_4CR)_8$ (**7**)	1927	2079	2.10	1.2	9.6	[68]
$Zn_3(ntb)_2$[h]			419	1.0	1		[90]
$Zn_3(bdt)_3$	$Zn_3(N_4CR)_6$ (**5**)	640		1.46	1.2	8.7	[76]
$Zn_3(OH)(p\text{-CDC})_{2.5}$	$Zn_3(\mu\text{-OH})(O_2CR)_5$ (**2**)		152	2.1	1	7.2	[91]
$Y_2(pdc)_3$	$Y(\mu\text{-}O_2CR)$ chains (**12**)	676		0.76	1		[92]
$Mo_3(btc)_2$	$Mo_2(O_2CR)_4$ (**1**)	1280	2010	1.75	1		[93]
$[In_3O(abtc)_{1.5}](NO_3)$	$In_3(\mu_3\text{-O})(O_2CR)_6$ (**4**)		1417	2.61	1.2	6.5	[94]
Dy(btc)	$Dy(\mu\text{-}O_2CR)$ chains (**13**)	655		1.32	1		[95]
$Er_2(pdc)_3$	$Er(\mu\text{-}O_2CR)$ chains (**12**)	427		0.68	1		[92]

[a] See also Table 2. [b] Abbreviations: btt = 1,3,5-benzenetristetrazolate; ndc = 2,6-naphthalenedicarboxylate; diPyNI = *N*,*N*′-di-(4-pyridyl)-1,4,5,8-naphthalenetetracarboxydiimide; btc = 1,3,5-benzenetricarboxylate; bdc = 1,4-benzenedicarboxylate; ntc = 1,4,5,8- naphthalenetetracarboxylate; bdt = 1,4-benzeneditetrazolate; tpt-3tz = 2,4,6-tris(*p*-phenyltetrazolate)-*s*-triazine; btb = 1,3,5-benzenetribenzoate; tatb = 4,4′,4″-s-triazine-2,4,6-triyl-tribenzoate; dhtp = 2,5-dihydroxyterephthalate; bptc = 3,3′,5,5′-biphenyltetracarboxylate; tptc = 3,3″,5,5″-terphenyltetracarboxylate; qptc = 3,3‴,5,5‴-quaterphenyltetracarboxylate; BPTriC = biphenyl-3,4′,5-tricarboxylate; tzi = 5-tetrazolylisophthalate; tpb-3tz = 1,3,5-tris(*p*-phenyltetrazolate)benzene; ntb = 4,4′4″-nitrilotribenzoate; *p*-CDC = 1,12-dihydroxycarbonyl-1,12-dicarba-*closo*-dodecaborane; pdc = pyridine-3,5-dicarboxylate; abtc = 3,3′,5,5′-azobenzenetetracarboxylate. [c] Obtained from the N_2 isotherm at 77 K. [d] Obtained from the O_2 isotherm at 77 K. [e] Desorption occurs with hysteresis. [f] DMF molecules occupy the Mn^{2+} Lewis acid sites. [g] Total H_2 adsorption. [h] Upon desolvation, Zn^{2+}-bound DMF molecules are replaced by neighboring carboxylate groups.

temperature H_2 adsorption in metal–organic frameworks were obtained with Zn_4O(1,3,5-benzenetribenzoate)$_2$ and Zn_4O(1,4-benzenedicarboxylate)$_3$, commonly known as MOF-177 and MOF-5, respectively. These compounds adsorb totals of 11 and 9.8 wt% of H_2 at 90 bar and 77 K, corresponding to 49 and 64 $g L^{-1}$, respectively.[66,67] As expected, the total adsorption capacity for MOF-5 increases almost linearly with pressure above 100 bar, and reaches 11.9 wt% and 79 $g L^{-1}$ at 180 bar and 77 K, thus exceeding the density of liquid H_2 at 20 K. However, the low adsorption enthalpy of approximately 5 $kJ mol^{-1}$ is responsible for a total room-temperature uptake of only 1.4 wt% and 8.1 $g L^{-1}$ at 90 bar.[67] By comparison, despite exhibiting a BET surface area of only 2057 $m^2 g^{-1}$, approximately half of the 3800 $m^2 g^{-1}$ value for MOF-5, $Mn_3[(Mn_4Cl)_3(btt)_8(CH_3OH)_{10}]_2$ displays a total room-temperature capacity of 1.5 wt% under identical

conditions.[55] Moreover, the volumetric capacity for the manganese framework is 50% higher than that of MOF-5, and at 12.1 $g\,L^{-1}$ it represents a 77% increase over the density of compressed H_2 under the same conditions.[68] These results suggest that new materials that combine the advantages of large surface areas and high binding energies are expected to demonstrate even more promising storage properties at room temperature. Such materials could be produced, for example, by using known building units with unsaturated metal centers, such as the Cu_2–paddlewheel and the square-planar Mn_4Cl clusters, and extending the length of the bridging ligands. Despite possible complications due to the formation of interpenetrated frameworks, this approach has succeeded in producing isomorphous frameworks with increasing surface areas.[85]

5. Strategies for Incorporating Unsaturated Metal Centers in Metal–Organic Frameworks

Three different strategies have been employed so far to introduce coordinatively unsaturated metal centers into metal–organic frameworks. Although many frameworks with exposed metal sites may display interesting hydrogen storage properties, relevant measurements have been reported for only those enumerated in Tables 2 and 3 and for a series of cyano-bridged microporous frameworks (see Section 5.1).

The most common method for achieving coordinative unsaturation involves the removal of metal-bound volatile species, which typically function as terminal ligands for the metals embedded within the porous framework. Two other methods have also been reported, and they involve either the incorporation of metal species within the organic bridging ligands, or the impregnation of a given framework with excess metal cations.

5.1. Metal Building Units with Coordinatively Unsaturated Centers through Solvent Removal

The most widely exploited method thus far involves the synthesis of solvated metal–organic frameworks, from which metal-bound solvent molecules, such as *N*,*N*-dimethylformamide, *N*,*N*-diethylformamide, water, or methanol, are removed to produce coordinatively unsaturated metal centers. Although a large number of different frameworks have been produced by using this technique, most are based on a relatively small number of metal building units. These building units are either small multinuclear metal clusters or metal chains bridged by carboxylate or tetrazolate groups.

Figure 4 displays the types of unsaturated metal clusters that have been found inside the metal–organic frameworks listed in Table 3. One of the most ubiquitous cluster motifs is the bimetallic tetracarboxylate paddlewheel unit $\{M_2(O_2CR)_4\}$ (**1**), which is frequently formed in reactions involving Cu^{2+} and Zn^{2+} cations. Each metal ion in **1** is coordinated by four carboxylate groups and a solvent molecule in a square-pyramidal geometry. Solvent molecules on each of the two ions can be removed to give open metal sites, as observed for example in $Cu_3(btc)_2$ and $Mo_3(btc)_2$. Another common carboxylate-bridged cluster is $\{M_3(\mu_3\text{-}O)(O_2CR)_6\}$ (**4**), an oxo-centered trigonal building unit, which in Table 3 is found in frameworks of Sc^{3+}, Cr^{3+}, $Fe^{2+/3+}$, Ni^{2+}, Al^{3+}, and In^{3+}. These frameworks can be synthesized under conditions mimicking

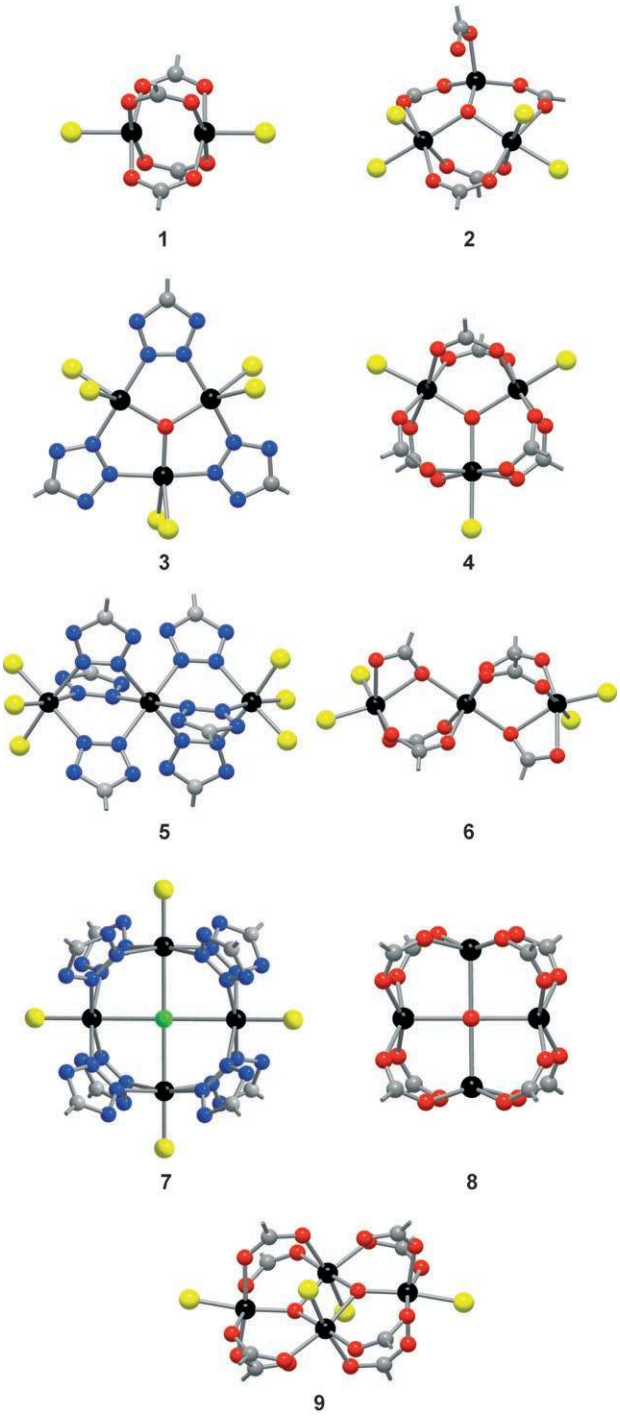

Figure 4. Structures of various clusters that function as building units for the metal–organic frameworks listed in Table 3, as determined by X-ray crystallography. Potential H_2 binding sites are shown as yellow spheres. Black, green, red, blue, and gray spheres represent metal, Cl, O, N, and C atoms, respectively.

those used for the formation of the geometrically analogous molecular clusters, which are known for an even wider variety of metal combinations.[96] Each metal ion in building unit **4** displays one potential H_2 binding site, as opposed to the linear trinuclear clusters $\{M_3(O_2CR)_6\}$ (**6**), in which two of the metal centers each present two possible H_2 binding sites. Cluster **4** and the oxo-centered square-planar cluster $\{M_4(\mu_4\text{-}O)(O_2CR)_8\}$ (**8**) have geometrically related tetrazolate-bridged analogues represented by the linear unit $\{M_3(N_4CR)_6\}$ (**5**) and the chloride-centered square-planar unit $\{M_4(\mu_4\text{-}Cl)(N_4CR)_8\}$ (**7**). The latter is featured in the sodalite-like framework $Mn_3[(Mn_4Cl)_3(btt)_8(CH_3OH)_{10}]_2$ and its Cu^{2+} analogue.

Less common are the hydroxo- and bis(μ-oxo)-bridged clusters $\{Zn_3(\mu\text{-}OH)(O_2CR)_5\}$ (**2**) and $\{Fe_4(\mu_3\text{-}O)_2(O_2CR)_8\}$ (**9**), which are only featured once each in Table 3. Also encountered only once thus far is the oxo-centered tetrazolate-bridged cluster $\{Cu_3(\mu_3\text{-}O)(N_4CR)_3\}$ (**3**), which was reported only recently in $Cu_6O(tzi)_3(NO_3)$, a rare example of a framework built from two types of unsaturated metal clusters. As opposed to the triangular carboxylate unit **4**, cluster **3** has only three bridging tetrazolate rings, and each metal displays a trigonal-bipyramidal geometry with two potential H_2 binding sites.

In addition to the frameworks in Table 2, materials based on selected clusters in Figure 4 exhibit some of the highest H_2 capacities for metal–organic frameworks. Among the materials that were investigated at high pressure, the isoreticular frameworks $Cu_2(bptc)$, $Cu_2(tptc)$, and $Cu_2(qptc)$ exhibit excess gravimetric H_2 capacities (excess capacity = uptake due to material only, not including uptake due to compression of gas in the empty volume) of 4.20, 6.06, and 6.07 wt% at 20 bar and 77 K.[85] High excess capacities were also reported for $Cr_3OF(bdc)_3$ and $Cu_3(BPTriC)$, which at 77 K adsorbed 6.1 and 5.7 wt% at 60 and 45 bar, respectively. The maximal adsorption enthalpies for these compounds, which include presumptive contributions from unsaturated Cr^{3+} and Cu^{2+} ions, respectively, are 10.0 and 7.3 kJ mol^{-1} and are among the highest known for microporous materials. Strong H_2 adsorption is also observed in $H_2[Co_4O(tatb)_{8/3}]$ and in $Cu_6O(tzi)_3(NO_3)$, for which zero-coverage adsorption enthalpy values of 10.1 and 9.5 kJ mol^{-1} have been attributed to H_2 binding to unsaturated Co^{2+} and Cu^{2+} centers, respectively. Although high-pressure data is not available for these compounds, relatively high capacities of 1.53 and 2.4 wt% were reported at 1 bar and 77 K for the cobalt and copper frameworks, respectively. Notable low-pressure capacities were also observed for $[In_3O(abtc)_{1.5}](NO_3)$ and $Fe_4O_2(btb)_{8/3}$, which adsorbed 2.61 and 2.1 wt% of H_2, respectively, at around 1 bar and 77 K.

The chains shown in Figure 5 constitute the inorganic building units for the remaining materials listed in Table 3. These motifs are far less common than the small multinuclear clusters discussed above. In fact, each of these chains is found in only one framework in Table 3, with the exception of the carboxylate-bridged chain **12**, which is featured in both $Y_2(pdc)_3$ and $Er_2(pdc)_3$. In contrast to the cluster-based materials, which normally display three-dimensional channels and have high surface areas and large micropore volumes, chain-based metal–organic frameworks typically exhibit one-

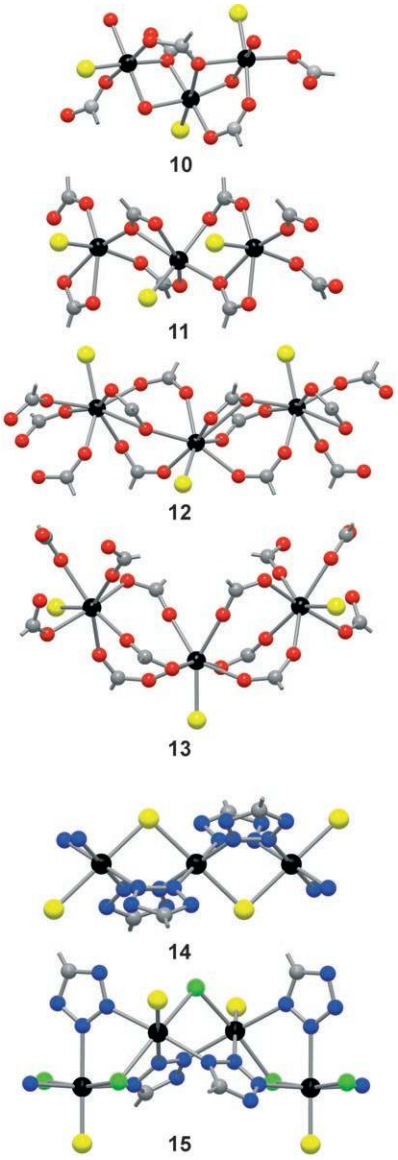

Figure 5. Partial structures of various chains that function as building blocks for metal–organic frameworks in which evacuation of solvent molecules can give rise to coordinatively unsaturated metal centers, as determined by X-ray crystallography. The solvent binding and potential H_2 binding sites are depicted as yellow spheres. Black, green, red, blue, and gray spheres represent metal, Cl, O, N, and C atoms, respectively.

dimensional channels that lead to low surface areas and reduced micropore volumes. As such, despite exhibiting a relatively high adsorption enthalpy of 8.8 kJ mol^{-1}, $Zn_2(dhtp)$ shows an H_2 capacity of only 2.8 wt% at 30 bar and 77 K, which is still the best value reported thus far for a chain-based microporous framework with coordinatively unsaturated metal sites.

Although themogravimetric analysis and powder X-ray diffraction data suggest that empty coordination sites may become available in the frameworks in Table 3, direct evidence for H_2 binding to these materials has not yet been reported, as the high temperature required to evacuate metal-bound solvent molecules can lead to loss of long-range

ordering and crystallinity. The low thermal stability of most frameworks thereby prevents the use of common neutron diffraction techniques, which could provide direct structural evidence of metal–H_2 binding. For example, although the adsorption enthalpies of 8.8, 8.7, and 8.4 kJ mol^{-1} reported for $Mn_2(bdt)Cl_2$, $Zn_3(bdt)_3$, and $Mn_3(bdt)_3$, respectively, were attributed to H_2 binding to Mn^{2+} and Zn^{2+} sites, the poor crystallinity of these frameworks prevented further studies of the presumed metal–H_2 binding interactions.

In other cases, as for example in $Mg_3(ndc)_3$ and Mn(ndc), desolvation is accompanied by rearrangements to different crystalline phases. Powder diffraction patterns for these desolvated phases differ from those of the as-synthesized materials, and unless crystals of the respective compounds remain single upon desolvation, identification of the rearranged structures is often difficult. The development of milder desolvation techniques is therefore necessary to allow further investigation of metal–H_2 binding in known materials. In addition, the synthesis of more thermally robust materials should provide new opportunities to study the metal–H_2 interaction and ultimately to devise principles for the design of improved hydrogen storage materials.

Cyano-bridged frameworks typically exhibit excellent crystallinity and are thus more amenable to neutron studies.[97] As in the metal–organic frameworks, coordinatively unsaturated metal sites become available in the cyanide-bridged materials upon careful evacuation of the metal-bound water molecules. One such example is the Prussian blue analogue $Cu_3[Co(CN)_6]_2$, for which low-temperature neutron diffraction revealed Cu^{2+}–D_2 interactions at increased D_2 loading.[64] Surprisingly, the related Prussian blue analogue $Mn_3[Co(CN)_6]_2$ did not exhibit Mn^{2+}–D_2 interactions even under increased D_2 loadings,[98] in contrast to the aforementioned results, indicating that isostructural sodalite-type compounds bind H_2 more strongly to Mn^{2+} centers than to Cu^{2+}.[55,65] The result is in line, however, with previous H_2 adsorption data for a series of Prussian blue analogues $M_3[Co(CN)_6]$, which exhibited maximal adsorption enthalpies of 5.9 kJ mol^{-1} for M = Mn^{2+} and 7.4 kJ mol^{-1} for M = Cu^{2+}.[97a] Hydrogen storage measurements for metal–cyanide frameworks with the general formula $A_2Zn_3[Fe(CN)_6]_2$ (A = alkali metal) have also allowed comparison of the H_2 binding strengths of H_3O^+, $Li(H_2O)^+$, Na^+, K^+, and Rb^+.[97e] The zero-coverage enthalpy of adsorption in these materials decreased in the order $K^+ > H_3O^+ > Rb^+ \approx Li(H_2O)^+ > Na^+$ and ranged from 9.0 kJ mol^{-1} for K^+ to 7.7 kJ mol^{-1} for Na^+.

5.2. Incorporating Coordinatively Unsaturated Metal Centers within the Organic Linkers

A second method for introducing unsaturated metal centers within metal–organic frameworks is to attach metal fragments to the organic bridging ligands. This could be accomplished, for example, by employing 2,2′-bipyridine-5,5′-dicarboxylate (H_2BipyDC) or similar metal chelating dicarboxylates or ditetrazolates as the bridging ligands. In contrast to the strategy described in Section 5.1, the unsaturated metal centers produced in this manner would not be part of the metal-building unit of a given framework and therefore their incorporation could be accomplished either prior to or after the synthesis of a given framework. At the same time, metal centers introduced by using this method would be more amenable to chemical modifications, which is particularly attractive because it implies that multiple metal–H_2 binding sites could become available by removing, for example, all four carbonyl ligands from a hypothetical bridging ligand $[(BipyDC)M(CO)_4]^{2-}$ (**16**; Figure 6). Although unsaturated metal sites have not been obtained yet with this ligand, porous metal–organic frameworks incorporating both metal-free, and metal-ligated $BipyDC^{2-}$ units have been reported.[99]

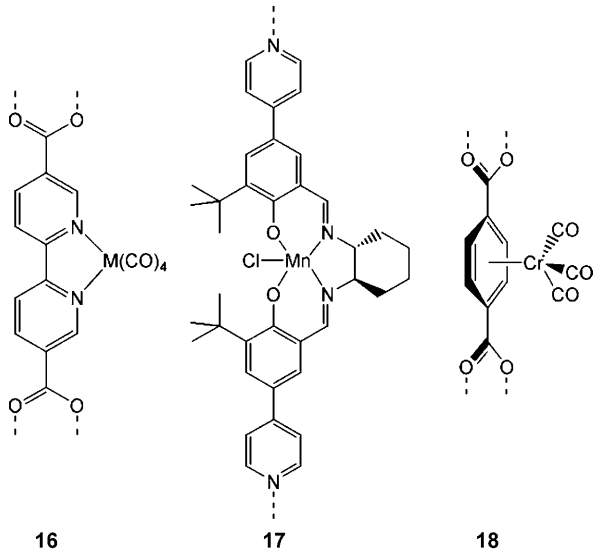

Figure 6. Molecular structures of bridging ligands bearing metal fragments that can give rise to metal–H_2 binding sites.

Chelated metal centers have also been isolated inside porous frameworks by using porphyrin-[100] and salen-type ligands (salen = *N*,*N*′-bis(salicylidene)ethylenediamine),[101] such as the salen–Mn^{3+} complex **17** (Figure 6). Complex **17** functions as a bridging ligand in a pillared Zn^{2+}-based framework,[101b] and although no H_2 uptake data is reported for this material, the Mn^{3+} ion can function as a Lewis acid catalyst, suggesting that it displays open coordination sites that could lead to strong H_2 adsorption. These and similar results reported by Suslick and co-workers for porphyrin-based frameworks[100] suggest that a metal–chelate-based strategy could lead to novel materials with interesting H_2 storage properties.

Indeed, an important result in this area was the incorporation of half-sandwich units {(bdc)$Cr(CO)_3$} (**18**) inside $Zn_4O(bdc)_3$.[102] Evacuation of all three CO molecules from {$Cr(CO)_3$} units in $Zn_4O[(bdc)Cr(CO)_3]_3$ was evidenced by thermogravimetric analysis, and framework integrity was confirmed by powder X-ray diffraction. However, a change from colorless to gray indicated the possible aggregation of Cr atoms at increased temperature, such that the adsorption capacity of this material reached only 0.2 molecules of H_2 per formula unit. Milder photolysis methods were therefore used

to decarbonylate $Zn_4O[(bdc)Cr(CO)_3]_3$, and infrared spectroscopy showed that $Zn_4O[(bdc)Cr(CO)_2(H_2)]_3$ and $Zn_4O[(bdc)Cr(CO)_2(N_2)]_3$ could be produced under UV light in atmospheres of H_2 and N_2, respectively. Unfortunately, the low efficiency of the photolysis in solid-state samples precluded further decarbonylation of these products, such that other, more efficient means to remove carbonyl ligands need to be developed to take advantage of all three metal binding sites on the half-sandwich units. Nevertheless, given that the H_2 binding energy for the hydrogenated species is expected to be in the vicinity of 60–70 kJ mol^{-1}, as measured for $[(C_6H_6)Cr(CO)_2(H_2)]$[26] and $[(C_6H_5Me)Cr(CO)_2(H_2)]$,[27] these results suggest that an approach involving the functionalization of the organic bridging ligands could produce materials with very high H_2 affinity.

5.3. Impregnation of Metal–Organic Frameworks with Metal Ions

A very recent development in the area of H_2 storage in metal–organic frameworks has been the use of ion exchange[68b] and metal impregnation techniques for stronger H_2 binding. For example, attempts to exchange the Mn^{2+} cations that balance the charge of the anionic framework in $Mn_3[(Mn_4Cl)_3(btt)_8(CH_3OH)_{10}]_2$ almost invariably resulted in the introduction of extra equivalents of metal chlorides to produce materials of the type $M_3[(Mn_4Cl)_3(btt)_8(CH_3OH)_{10}]_2{\cdot}x\,MCl_2$ ($M = Fe^{2+}$, Co^{2+}, Ni^{2+}, Cu^{2+}, Zn^{2+}; $x = 0$–2).[68a] As shown in Table 3, these new materials exhibit a large variation in the zero-coverage H_2 adsorption enthalpy, ranging from 8.5 kJ mol^{-1} for the Cu^{2+}-exchanged framework to 10.5 kJ mol^{-1} for the Co^{2+}-exchanged phase. The latter represents the highest value reported thus far for a microporous metal–organic framework.

Employing a different approach, Mulfort and Hupp used a suspension of Li metal in DMF to reduce $Zn_2(ndc)_2(diPyNI)$, a metal–organic framework with a pillared structure.[69] This procedure allowed doping of the as-synthesized material with approximately 5 mol % of Li^+ cations, resulting in a remarkable increase in the H_2 adsorption capacity from 0.93 to 1.63 wt. % at 77 K and 1 atm. The calculated isosteric enthalpy of adsorption also showed an increase from the as-synthesized material over the entire H_2 loading range. The zero-coverage H_2 binding energy in this Li^+-doped material was a modest 6.1 kJ mol^{-1}, which is nevertheless in good agreement with previous measurements for Li^+-exchanged zeolites.[11–13] Despite the scarcity of examples that demonstrate the metal impregnation strategy, the two examples reported thus far are encouraging and suggest that other materials can be modified in a similar manner to produce microporous frameworks with an enhanced hydrogen affinity.

6. Conclusion and Outlook

Microporous metal–organic frameworks are promising hydrogen storage materials, and the isolation of unsaturated metal ions can be used as a systematic way to increase the H_2 binding affinity. Although many known frameworks may display metal–H_2 interactions, very few experiments have been performed to test this assumption. Critical areas that are likely to produce better results or improve on the ones reported so far are the elucidation of milder methods to desolvate metals within the pores and the synthesis of more robust frameworks that can maintain crystallinity during the thermal evacuation of metal-bound solvent molecules. Possible desolvation strategies for thermally sensitive frameworks may include microwave or photolytic evacuation methods. In turn, the development of new ligands with metal-binding groups that form stronger metal–ligand bonds should lead to materials with increased thermal stability. Another possible strategy that could yield metal–organic frameworks with increased H_2 affinity involves the incorporation of a larger concentration of charged sites within the pores. This could be achieved either by the use of multi-anionic bridging ligands, which should increase the number of metal atoms per formula unit, or by the incorporation of negative charges, which can also interact electrostatically with the H_2 quadrupole.

Overall, very encouraging results have been reported in a relatively short time, and a few new strategies to obtain unsaturated metal centers were developed only within the last year. Moreover, some of the results reported thus far show that metal–organic frameworks can meet most of the 2010 DoE targets on a materials basis when operating at 77 K. These allow researchers in the area to be optimistic when faced with the challenge of increasing the H_2 binding energy to produce a hydrogen storage system that will ultimately function near ambient temperature.

Addendum

Two very recent reports have demonstrated strong interactions between H_2 and exposed metal sites within metal–organic frameworks. An isosteric heat of adsorption of 12.3 kJ mol^{-1} was reported for $Zn_3(bdc)_3[Cu(pyen)]$ ($pyenH_2$ = 5-methyl-4-oxo-1,4-dihydropyridine-3-carbaldehyde)[104] and an initial adsorption enthalpy of 13.5 kJ mol^{-1} was established for $Ni_2(dhtp)$ by using variable-temperature infrared spectroscopy.[105]

We thank the US Department of Energy and General Motors Corporation for funding.

Received: March 11, 2008
Published online: August 8, 2008

[1] a) A. Züttel, *Naturwissenschaften* **2004**, *91*, 157; b) A. M. Seayad, D. M. Antonelli, *Adv. Mater.* **2004**, *16*, 765; c) B. Sakintuna, F. Lamari-Darkrim, M. Hirscher, *Int. J. Hydrogen Energy* **2007**, *32*, 1121; d) S.-i. Orimo, Y. Nakamori, J. R. Eliseo, A. Zuttel, C. M. Jensen, *Chem. Rev.* **2007**, *107*, 4111; e) M. Felderhoff, C. Weidenthaler, R. von Helmolt, U. Eberle, *Phys. Chem. Chem. Phys.* **2007**, *9*, 2643, and references therein.

[2] a) J. A. R. Navarro, E. Barea, J. M. Salas, N. Masciocchi, S. Galli, A. Sironi, C. O. Ania, J. B. Parra, *Inorg. Chem.* **2006**, *45*, 2397; b) X. Lin, J. Jia, P. Hubberstey, M. Schroder, N. R.

Champness, *CrystEngComm* **2007**, *9*, 438; c) D. J. Collins, H. C. Zhou, *J. Mater. Chem.* **2007**, *17*, 3154, and references therein.
[3] a) X. Zhao, B. Xiao, A. J. Fletcher, K. M. Thomas, D. Bradshaw, M. J. Rosseinsky, *Science* **2004**, *306*, 1012; b) C. Yang, X. Wang, M. A. Omary, *J. Am. Chem. Soc.* **2007**, *129*, 15454.
[4] Hydrogen, Fuel Cells and Infrastructure Technologies Program: Multi-Year Research, Development, and Demonstration Plan: Planned Program Activities for 2005–2015, website address (February 2008): http://www1.eere.energy.gov/hydrogenandfuelcells/mypp/.
[5] S. K. Bhatia, A. L. Myers, *Langmuir* **2006**, *22*, 1688.
[6] *Activation of Small Molecules* (Ed.: W. B. Tolman), Wiley-VCH, Weinheim, **2006**.
[7] G. J. Kubas, R. R. Ryan, B. I. Swanson, P. J. Vergamini, H. J. Wasserman, *J. Am. Chem. Soc.* **1984**, *106*, 451.
[8] a) G. J. Kubas, R. R. Ryan, D. Wrobleski, *J. Am. Chem. Soc.* **1986**, *108*, 1339; b) G. J. Kubas, C. J. Unkefer, B. I. Swanson, E. Fukushima, *J. Am. Chem. Soc.* **1986**, *108*, 7000.
[9] a) G. J. Kubas *Metal Dihydrogen and σ-Bond Complexes—Structure, Theory, and Reactivity*, Kluwer-Academic/Plenum Publishers, New York, **2001**; b) G. J. Kubas, *Chem. Rev.* **2007**, *107*, 4152.
[10] A. Zecchina, S. Bordiga, J. G. Vitillo, G. Ricchiardi, C. Lamberti, G. Spoto, M. Bjørgen, K. P. Lillerud, *J. Phys. Chem.* **2005**, *127*, 6361.
[11] C. H. Wu, *J. Chem. Phys.* **1979**, *71*, 783.
[12] C. Otero Areán, O. V. Manoilova, B. Bunelli, M. Rodríguez Delgado, G. Turnes Palomino, E. Garrone, *Chem. Phys. Lett.* **2003**, *370*, 631.
[13] C. Otero Areán, D. Nachtigallova, P. Nachtigall, E. Garrone, M. Rodríguez Delgado, *Phys. Chem. Chem. Phys.* **2007**, *9*, 1421.
[14] J. E. Bushnell, P. R. Kemper, M. T. Bowers, *J. Phys. Chem.* **1994**, *98*, 2044.
[15] C. Otero Areán, M. Rodríguez Delgado, G. Turnes Palomino, M. Tomás Rubio, N. M. Tsyganenko, A. A. Tsyganenko, E. Garrone, *Microporous Mesoporous Mater.* **2005**, *80*, 247.
[16] G. Ricchiardi, J. G. Vitillo, D. Cocina, E. N. Gribov, A. Zecchina, *Phys. Chem. Chem. Phys.* **2007**, *9*, 2753.
[17] E. N. Gribov, S. Bertarione, D. Scarano, C. Lamberti, G. Spoto, A. Zecchina, *J. Phys. Chem. B* **2004**, *108*, 16174.
[18] G. Turnes Palomino, M. R. Llop Carayol, C. Otero Areán, *J. Mater. Chem.* **2006**, *16*, 2884.
[19] J. E. Bushnell, P. R. Kemper, P. Maître, M. T. Bowers, *J. Am. Chem. Soc.* **1994**, *116*, 9710.
[20] J. E. Bushnell, P. Maître, P. R. Kemper, M. T. Bowers, *J. Chem. Phys.* **1997**, *106*, 10153.
[21] J. E. Bushnell, P. R. Kemper, M. T. Bowers, *J. Phys. Chem.* **1993**, *97*, 11628.
[22] M. W. George, M. T. Haward, R. A. Hamley, C. Hughes, F. P. A. Johnson, V. K. Popov, M. Poliakoff, *J. Am. Chem. Soc.* **1993**, *115*, 2286.
[23] P. R. Kemper, P. Weis, M. T. Bowers, *Int. J. Mass Spectrom. Ion Proc.* **1997**, *160*, 17.
[24] J. R. Wells, P. G. House, E. Weitz, *J. Phys. Chem.* **1994**, *98*, 8343.
[25] E. F. Walsh, V. K. Popov, M. W. George, M. Poliakoff, *J. Phys. Chem.* **1995**, *99*, 12016.
[26] E. F. Walsh, M. W. George, S. Goff, S. M. Nikiforov, V. K. Popov, X.-Z. Sun, M. Poliakoff, *J. Phys. Chem.* **1996**, *100*, 19425.
[27] S. M. Howdle, M. A. Healy, M. Poliakoff, *J. Am. Chem. Soc.* **1990**, *112*, 4804.
[28] J. M. Millar, R. V. Kastrup, M. T. Melchior, I. T. Horvath, C. D. Hoff, R. H. Crabtree, *J. Am. Chem. Soc.* **1990**, *112*, 9643.
[29] P. Weis, P. R. Kemper, M. T. Bowers, *J. Phys. Chem. A* **1997**, *101*, 2809.
[30] J. E. Bushnell, P. R. Kemper, M. T. Bowers, *J. Phys. Chem.* **1995**, *99*, 15602.
[31] P. R. Kemper, J. E. Bushnell, G. von Helden, M. T. Bowers, *J. Phys. Chem.* **1993**, *97*, 52.
[32] C. J. Carpenter, P. A. M. van Koppen, P. R. Kemper, J. E. Bushnell, P. Weis, J. K. Perry, M. T. Bowers, *Int. J. Mass Spectrom.* **2003**, *230*, 161.
[33] P. R. Kemper, P. Weis, M. T. Bowers, *Chem. Phys. Lett.* **1998**, *293*, 503.
[34] P. R. Kemper, P. Weis, M. T. Bowers, P. Maître, *J. Am. Chem. Soc.* **1998**, *120*, 13494.
[35] M. J. Manard, J. E. Bushnell, S. L. Bernstein, M. T. Bowers, *J. Phys. Chem. A* **2002**, *106*, 10027.
[36] S. Bordiga, L. Regli, F. Bonino, E. Groppo, C. Lamberti, B. Xiao, P. S. Wheatley, R. E. Morris, A. Zecchina, *Phys. Chem. Chem. Phys.* **2007**, *9*, 2676.
[37] J. E. Bushnell, P. R. Kemper, P. van Koppen, M. T. Bowers, *J. Phys. Chem. A* **2001**, *105*, 2216.
[38] A. A. Gonzalez, C. D. Hoff, *Inorg. Chem.* **1989**, *28*, 4295.
[39] D. M. Gusev, A. B. Vymenits, V. I. Bakhmutov, *Inorg. Chem.* **1992**, *31*, 1.
[40] V. I. Bakhmutov, J. Bertran, M. A. Esteruelas, A. Lledos, F. Maseras, J. Modrego, L. A. Oro, E. Sola, *Chem. Eur. J.* **1996**, *2*, 815.
[41] V. I. Bakhmutov, E. V. Vorontsov, A. B. Vymenits, *Inorg. Chem.* **1995**, *34*, 214.
[42] B. E. Hauger, D. Gusev, K. G. Caulton, *J. Am. Chem. Soc.* **1994**, *116*, 208.
[43] R. H. Crabtree, M. Lavin, L. Bonneviot, *J. Am. Chem. Soc.* **1986**, *108*, 4032.
[44] Y.-I. Ishikawa, P. A. Hackett, D. M. Rayner, *J. Phys. Chem.* **1989**, *93*, 652.
[45] A. A. Gonzalez, K. Zhang, S. P. Nolan, R. L. de La Vega, S. L. Mukerjee, C. D. Hoff, G. J. Kubas, *Organometallics* **1988**, *7*, 2429.
[46] A. A. Gonzalez, K. Zhang, S. L. Mukerjee, C. D. Hoff, G. R. K. Khalsa, G. J. Kubas, *ACS Symp. Ser.* **1990**, *428*, 133.
[47] K. Christmann, *Surf. Sci. Rep.* **1988**, *9*, 1.
[48] a) A. Dedieu, *Chem. Rev.* **2000**, *100*, 543; b) G. Frenking, N. Fröhlich, *Chem. Rev.* **2000**, *100*, 717; c) S. Niu, M. B. Hall, *Chem. Rev.* **2000**, *100*, 353; d) M. Torrent, M. Solà, G. Frenking, *Chem. Rev.* **2000**, *100*, 439.
[49] R. C. Lochan, M. Head-Gordon, *Phys. Chem. Chem. Phys.* **2006**, *8*, 1357.
[50] a) O. Sun, Q. Wang, P. Jena, Y. Kawazoe, *J. Am. Chem. Soc.* **2005**, *127*, 14582; b) Q. Sun, P. Jena, Q. Wang, M. Marquez, *J. Am. Chem. Soc.* **2006**, *128*, 9741; c) K. R. S. Chandrakumar, S. K. Ghosh, *Nano Lett.* **2008**, *8*, 13.
[51] A. Blomqvist, C. Moysés Araújo, P. Srepusharawoot, R. Ahuja, *Proc. Natl. Acad. Sci. USA* **2007**, *104*, 20173.
[52] a) Q. Yang, C. Zhong, *J. Phys. Chem. B* **2006**, *110*, 655; b) Y. Y. Sun, Y. H. Kim, S. B. Zhang, *J. Am. Chem. Soc.* **2007**, *129*, 12606; c) J. L. Belof, A. C. Stern, M. Eddaoudi, B. Space, *J. Am. Chem. Soc.* **2007**, *129*, 15202.
[53] C. Prestipino, L. Regli, J. G. Vitillo, F. Bonino, A. Damin, C. Lamberti, A. Zecchina, P. L. Solari, K. O. Kongshaug, S. Bordiga, *Chem. Mater.* **2006**, *18*, 1337.
[54] V. K. Peterson, Y. Liu, C. M. Brown, C. J. Kepert, *J. Am. Chem. Soc.* **2006**, *128*, 15578.
[55] M. Dincă, A. Dailly, Y. Liu, C. M. Brown, D. A. Neumann, J. R. Long, *J. Am. Chem. Soc.* **2006**, *128*, 16876.
[56] J. L. C. Rowsell, O. M. Yaghi, *J. Am. Chem. Soc.* **2006**, *128*, 1304.
[57] P. M. Forster, J. Eckert, B. D. Heiken, J. B. Parise, J. W. Yoon, S. H. Jhung, J.-S. Chang, A. K. Cheetham, *J. Am. Chem. Soc.* **2006**, *128*, 16846.
[58] N. Guillou, Q. Gao, P. M. Forster, J.-S. Chang, M. Noguès, S.-E. Park, G. Férey, *Angew. Chem.* **2001**, *113*, 2913; *Angew. Chem. Int. Ed.* **2001**, *40*, 2831.

[59] P. M. Forster, J. Eckert, J.-S. Chang, S.-E. Park, G. Férey, A. K. Cheetham, *J. Am. Chem. Soc.* **2003**, *125*, 1309.
[60] A. G. Wong-Foy, A. J. Matzger, O. M. Yaghi, *J. Am. Chem. Soc.* **2006**, *128*, 3494.
[61] J.-Y. Lee, J. Li, J. Jagiello, *J. Solid State Chem.* **2005**, *178*, 2527.
[62] B. Xiao, P. S. Wheatley, X. Zhao, A. J. Fletcher, S. Fox, A. G. Rossi, I. L. Megson, S. Bordiga, L. Regli, K. M. Thomas, R. E. Morris, *J. Am. Chem. Soc.* **2007**, *129*, 1203.
[63] B. Panella, M. Hirscher, H. Pütter, U. Müller, *Adv. Funct. Mater.* **2006**, *16*, 520.
[64] M. R. Hartman, V. K. Peterson, Y. Liu, S. S. Kaye, J. R. Long, *Chem. Mater.* **2006**, *18*, 3221.
[65] M. Dincă, W. S. Han, Y. Liu, A. Dailly, C. M. Brown, J. R. Long, *Angew. Chem.* **2007**, *119*, 1441; *Angew. Chem. Int. Ed.* **2007**, *46*, 1419.
[66] H. Furukawa, M. A. Miller, O. M. Yaghi, *J. Mater. Chem.* **2007**, *17*, 3197.
[67] S. S. Kaye, A. Dailly, O. M. Yaghi, J. R. Long, *J. Am. Chem. Soc.* **2007**, *129*, 14176.
[68] a) M. Dincă, J. R. Long, *J. Am. Chem. Soc.* **2007**, *129*, 11172; b) Y. Liu, V. C. Kravtsov, R. Larsen, M. Eddaoudi, *Chem. Commun.* **2006**, 1488.
[69] K. L. Mulfort, J. T. Hupp, *J. Am. Chem. Soc.* **2007**, *129*, 9604.
[70] M. Dincă, J. R. Long, *J. Am. Chem. Soc.* **2005**, *127*, 9376.
[71] I. Senkovska, S. Kaskel, *Eur. J. Inorg. Chem.* **2006**, 4654.
[72] T. Loiseau, L. Lecroq, C. Volkringer, J. Marrot, G. Férey, M. Haouas, F. Taulelle, S. Bourrelly, P. L. Llewellyn, M. Latroche, *J. Am. Chem. Soc.* **2006**, *128*, 10223.
[73] M. Latroche, S. Surblé, C. Serre, C. Mellot-Draznieks, P. L. Llewellyn, J.-H. Lee, J.-S. Chang, S. H. Jhung, G. Férey, *Angew. Chem.* **2006**, *118*, 8407; *Angew. Chem. Int. Ed.* **2006**, *45*, 8227.
[74] G. Férey, C. Mellot-Draznieks, C. Serre, F. Millange, J. Dutour, S. Surblé, I. Margiolaki, *Science* **2005**, *309*, 2040.
[75] S. Surblé, F. Millange, C. Serre, T. Düren, M. Latroche, S. Bourrelly, P. L. Llewellyn, G. Férey, *J. Am. Chem. Soc.* **2006**, *128*, 14889.
[76] M. Dincă, A. F. Yu, J. R. Long, *J. Am. Chem. Soc.* **2006**, *128*, 8904.
[77] H. R. Moon, N. Kobayashi, M. P. Suh, *Inorg. Chem.* **2006**, *45*, 8672.
[78] M. Dincă, A. Dailly, C. Tsay, J. R. Long, *Inorg. Chem.* **2008**, *47*, 11.
[79] S. B. Choi, M. J. Seo, M. Cho, Y. Kim, M. K. Jin, D.-Y. Jung, J.-S. Choi, W.-S. Ahn, J. L. C. Rowsell, J. Kim, *Cryst. Growth Des.* **2007**, *7*, 2290.
[80] J. H. Yoon, S. B. Choi, Y. J. Oh, M. J. Seo, Y. H. Joon, T.-B. Lee, D. Kim, S. H. Choi, J. Kim, *Catal. Today* **2007**, *120*, 324.
[81] S. Ma, H.-C. Zhou, *J. Am. Chem. Soc.* **2006**, *128*, 11734.
[82] P. D. C. Dietzel, B. Panella, M. Hirscher, R. Blom, H. Fjellvåg, *Chem. Commun.* **2006**, 959.
[83] S. Ma, X.-S. Wang, E. S. Manis, C. D. Collier, H.-C. Zhou, *Inorg. Chem.* **2007**, *46*, 3432.
[84] B. Chen, N. W. Ockwig, A. R. Millward, D. S. Contreras, O. M. Yaghi, *Angew. Chem.* **2005**, *117*, 4823; *Angew. Chem. Int. Ed.* **2005**, *44*, 4745.
[85] X. Lin, J. Jia, X. Zhao, K. M. Thomas, A. J. Blake, G. S. Walker, N. R. Champness, R. Hubberstey, M. Schröder, *Angew. Chem.* **2006**, *118*, 7518; *Angew. Chem. Int. Ed.* **2006**, *45*, 7358.
[86] S. Ma, D. Sun, M. Ambrogio, J. A. Fillinger, S. Parkin, H.-C. Zhou, *J. Am. Chem. Soc.* **2007**, *129*, 1858.
[87] D. Sun, S. Ma, Y. Ke, J. D. Collins, H.-C. Zhou, *J. Am. Chem. Soc.* **2006**, *128*, 3896.
[88] A. G. Wong-Foy, O. Lebel, A. J. Matzger, *J. Am. Chem. Soc.* **2007**, *129*, 15740.
[89] F. Nouar, J. F. Eubank, T. Bousquet, L. Wojtas, M. J. Zaworotko, M. Eddaoudi, *J. Am. Chem. Soc.* **2008**, *130*, 1833.
[90] Y. E. Cheon, E. Y. Lee, M. P. Suh, *Chem. Eur. J.* **2007**, *13*, 4208.
[91] O. K. Farha, A. M. Spokoyny, K. L. Mulfort, M. F. Hawthorne, C. A. Mirkin, J. T. Hupp, *J. Am. Chem. Soc.* **2007**, *129*, 12680.
[92] J. Jia, X. Lin, A. J. Blake, N. R. Champness, P. Hubberstey, L. Shao, G. Walker, C. Wilson, M. Schröder, *Inorg. Chem.* **2006**, *45*, 8838.
[93] M. Kramer, U. Schwarz, S. Kaskel, *J. Mater. Chem.* **2006**, *16*, 2245.
[94] Y. Liu, J. F. Eubank, A. J. Cairns, J. Eckert, V. C. Kravtsov, R. Luebke, M. Eddaoudi, *Angew. Chem.* **2007**, *119*, 3342; *Angew. Chem. Int. Ed.* **2007**, *46*, 3278.
[95] X. Guo, G. Zhu, Z. Li, F. Sun, Z. Yang, S. Qiu, *Chem. Commun.* **2006**, 3172.
[96] R. C. Mehrotra, R. Bohra, *Metal Carboxylates*, Academic Press Inc. London, **1983**.
[97] a) S. S. Kaye, J. R. Long, *J. Am. Chem. Soc.* **2005**, *127*, 6506; b) K. W. Chapman, P. D. Southon, C. L. Weeks, C. J. Kepert, *Chem. Commun.* **2005**, 3322; c) J. T. Culp, C. Matranga, M. Smith, E. W. Bittner, B. Bockrath, *J. Phys. Chem. B* **2006**, *110*, 8325; d) S. Natesakhawat, J. T. Culp, C. Matranga, B. Bockrath, *J. Phys. Chem. C* **2007**, *111*, 1055; e) S. S. Kaye, J. R. Long, *Chem. Commun.* **2007**, 4486.
[98] K. W. Chapman, P. J. Chupas, E. R. Maxey, J. W. Richardson, *Chem. Commun.* **2006**, 4013.
[99] a) E. Y. Lee, M. P. Suh, *Angew. Chem.* **2004**, *116*, 2858; *Angew. Chem. Int. Ed.* **2004**, *43*, 2798; b) G.-L. Law, K.-L. Wong, Y.-Y. Yang, Q.-Y. Yi, G. Jia, W.-T. Wong, P. A. Tanner, *Inorg. Chem.* **2007**, *46*, 9754; c) K. C. Szeto, K. O. Kongshaug, S. Jakobsen, M. Tilset, K. P. Lillerud, *Dalton Trans.* **2008**, 2054.
[100] a) M. E. Kosal, J.-H. Chou, S. R. Wilson, K. S. Suslick, *Nat. Mater.* **2002**, *1*, 118; b) D. W. Smithenry, S. R. Wilson, K. S. Suslick, *Inorg. Chem.* **2003**, *42*, 7719; c) K. S. Suslick, P. Bhyrappa, J.-H. Chou, M. E. Kosal, S. Nakagaki, B. W. Smithenry, S. R. Wilson, *Acc. Chem. Res.* **2005**, *38*, 283.
[101] a) R. Kitaura, G. Onoyama, H. Sakamoto, R. Matsuda, S.-i. Noro, S. Kitagawa, *Angew. Chem.* **2004**, *116*, 2738; *Angew. Chem. Int. Ed.* **2004**, *43*, 2684; b) S.-H. Cho, B. Ma, S. T. Nguyen, J. T. Hupp, T. Albrecht-Schmitt, *Chem. Commun.* **2006**, 2563.
[102] S. S. Kaye, J. R. Long, *J. Am. Chem. Soc.* **2008**, *130*, 806.
[103] Y. Liu, H. Kabbour, C. M. Brown, D. A. Neumann, C. C. Ahn, *Langmuir* **2008**, *24*, 4772.
[104] B. Chen, X. Zhao, A. Putkham, K. Hong, E. B. Lobkovsky, E. J. Hurtado, A. J. Fletcher, K. M. Thomas, *J. Am. Chem. Soc.* **2008**, *130*, 641.
[105] J. G. Vitillo, L. Regli, S. Chavan, G. Ricchiardi, G. Spoto, P. D. C. Dietzel, S. Bordiga, A. Zecchina, *J. Am. Chem. Soc.* **2008**, *130*, 8386.

